A Software Package for an Adaptive Satellite-based Sampling for Oceanographic cruises (SPASSOv2.0): tracking fine scale features for physical and biogeochemical studies

Louise Rousselet, Francesco d'Ovidio, Lloyd Izard, Alice Della Penna, Anne Petrenko, Stéphanie Barrillon, Francesco Nencioli, Andrea M. Doglioli

A Software Package for an Adaptive Satellite-based Sampling for Oceanographic cruises (SPASSOv2.0): tracking *fine scale* features for physical and biogeochemical studies.

Louise Rousselet[a] , Francesco d'Ovidio[a] , Lloyd Izard[a] , Alice Della-Penna[c,c2] , Anne Petrenko[b] , Stéphanie Barrillon[b] , Francesco Nencioli[d] , Andrea Doglioli[b]

[a] *Sorbonne Université, CNRS, IRD, MNHN, Laboratoire d'Océanographie et du Climat: Expérimentations et Approches Numériques (LOCEAN-IPSL), Paris, France*

[b] *Aix Marseille Univ., Université de Toulon, CNRS, IRD, MIO UM 110, 13288, Marseille, France*

[c] *Institute of Marine Science, University of Auckland, New Zealand* [c2] *School of Biological Sciences, University of Auckland, New Zealand* [d] *CLS, 11 Rue Hermès, Ramonville-Saint-Agne, 31520, France*

Corresponding author: Louise Rousselet, louise.rousselet@locean.ipsl.fr

ABSTRACT: During the past decade increasing interests arose in understanding the role of fine-scales (processes of the order of 10s of km) on ocean energy and biogeochemical budgets. However, *in situ* evidence of these processes remains poorly documented and represents only few specific ocean conditions. To fill this gap, new adaptive sampling feature-oriented strategies need to be developed. A possible approach is to target fine-scale features, identified from space, with *in situ* surveys. The SPASSO (Software Package for an Adaptive Satellite-based Sampling for Oceanographic cruises) package provides real-time analysis of satellite-derived products and diagnostics to identify fine-scale biophysical dynamics of any given study area. Besides the visualization of satellite products, the software computes a large variety of Eulerian and Lagrangian diagnostics inferred from near-real time altimetry to accurately direct oceanographic sampling towards fine-scale features. Over the last decade, this adaptive sampling methodology was successfully developed as showcased by several previous cruise examples. In 2023, the groundbreaking SWOT mission fosters the development of a new, improved and fully automated version of the software (SPASSOv2.0) to address the need to target SWOT-scales during *in situ* experiments.

1. Introduction

Ocean dynamics play a key role in the Earth system by distributing properties and matter around the globe. Ocean processes span a wide range of spatio-temporal scales from the global thermohaline circulation (~ years - hundreds of kilometers) to the microscale of turbulent mixing (~ hours/minutes - meters). In between stands the mesoscale (~ months - hundred kilometers) and submesoscale (~ days - few kilometers) dynamics characterized by the formation, transport and dissipation of features such as eddies, meanders, filaments or fronts (McWilliams 2006). These two regimes are closely associated, being defined by their transient nature as well as by respectively a dominant or non-negligible role of geostrophy (Lévy et al. 2012) and therefore nowadays often referred together as the *fine scale*. The *fine scales* have a central role in the physical, biogeochemical, and ecological dynamics of the ocean, strongly modulating in the horizontal and vertical the energy and transport pathways of the ocean, the exchanges at its interfaces, and shaping the dynamical "seascape" in which marine biota live (Kavanaugh et al. 2016; Mahadevan 2016; McGillicuddy Jr 2016; Taylor and Thompson 2023). Although empirical evidence of strong intermittent ocean circulation below Θ(100km) emerged since the 60s (e.g., Gill et al. 1974; Wyrtki et al. 1976), eddies and filaments still present today a major challenge in terms of their observability. During their life cycle, these structures may drift on distances that make several times their horizontal dimension. An observational network capable of fully resolving the spatial and temporal variability of one of these structures should therefore offer a precision of less than 1 km in the horizontal, of few meters in the vertical, on a region hundreds of kilometer large and hundreds of meter deep, for a period up to several months.

In the 1980's the first interdisciplinary studies based on *in situ* observation specifically focused on mesoscale features were carried out in the North Atlantic in the vicinity of the Gulf Stream and well-known Gulf Stream rings. Several mesoscale *in situ* mappings, such as the POLYGONE (Brekhovskikh et al. 1971), POLYMODE (McWilliams et al. 1983), MODE (Group et al. 1978) and Tourbillon (Tourbillon 1983) experiments were conducted in about 100 $\times$ 100 km areas, chosen ahead the field experiment for their intense mesoscale activity. At that time sampling strategies usually consisted in large scale surveys of the mapping area including CTD, expendable bathythermographs (XBT) profiles and floats deployment on a nearly uniform grid to target as precisely as possible the location of mesoscale features. After the completion of such large scale

survey, some higher resolution feature-oriented mapping was performed to observe fine-scale characteristics of a specific mesoscale feature.

At the same time, advances in satellite infrared imagery allowed for mapping large areas of sea surface temperature (SST). These near-real time images proved to be very useful for mesoscale feature identification and tracking, as thermal signature reveals the formation and circulation of warm and cold rings. Indeed several pioneering *in situ* cruises determined their sampling location and strategy using advanced very high resolution radiometer (AVHRR) data. The "Ring group" used these images to identify, track and sample several Gulf Stream cold rings for about a year (including four cruises) to describe both the physical and biological interactions during the rings' lifetime (Ring Group 1981). Similarly warm-core eddies in the Gulf of Mexico (Biggs 1992) and Algerian eddies in the Mediterranean Sea (Millot et al. 1997; Taupier-Letage et al. 2003) have been chosen from infrared images to study the mesoscale feature properties and associated phytoplankton dynamics. However, the success of such strategies relied on the availability of exploitable (i.e. cloud-free) sets of images.

This limitation is partially overcome since the 2000's thanks to the emergence of altimetry derived products (sea surface height (SSH) and surface velocities). This technology provide global observation of the ocean surface dynamics at mesoscale resolution ($\sim$ 75-100 km; Abdalla et al. 2021). In parallel, the first ocean color images (chlorophyll concentration, Chl) revealed clear biological mesoscale patterns (McClain 2009). The spectacular advances in remote sensing observations both in terms of horizontal resolution and temporal data availability widened the mesoscale feature detection capabilities. Indeed not only satellite-derived data were made available over the entire globe in a quasi near-real time, offering the possibility to track features directly from space, but also the variety of satellite products extensively diversified the approaches to identify mesoscale processes. While some spatial technologies provide cloud-free snapshots of mesoscale features (altimetry or micro-wave SST), others offer the opportunity, when sky is clear, to observe submesoscale heterogeneity by highlighting local tracer gradients at remarkable scales of few meters to kilometers (infra-red SST or ocean color). The submesoscale nature of phytoplankton patchiness, as seen by satellite-derived Chl, results from advection and stirring effect of small-scale ocean circulation as shown by several studies (Gower et al. 1980; Peláez and McGowan 1986; Mahadevan and Campbell 2002; d'Ovidio et al. 2010).

The *fine scale* surface transport information provided by satellite-derived products can be supplemented by Eulerian and Lagrangian analysis inferred from velocity fields. Eulerian diagnostics, such as kinetic energy (KE) or Okubo-Weiss (OW) criterion analyze local properties of the flow from instantaneous snapshot of the velocity field (Okubo 1970; Weiss 1991). On the other hand, Lagrangian diagnostics provide a finer measure of the dynamics experienced by a water parcel transported by a time-dependent flow field. By essence, the chaotic advection of water parcels reveals transport structures below the resolution of the velocity field. This is achieved by estimating sub-grid tracer filaments that are produced by the resolved features of the velocity field through stirring. For instance, a field of eddies with radii of 100 km and resolved at a resolution of 10 km can be used to initialize a Lagrangian model at 1 km resolution, and stir a numerical tracer into filaments at this finer resolution. This characteristic makes Lagrangian diagnostics powerful tools to investigate *fine scale* processes (d'Ovidio et al. 2009). For instance, the finite-size or finite-time Lyapunov exponents (FSLEs and FTLEs), a widely used Lagrangian diagnostic measuring the dispersal rate of advected particles, were proved to compare well with fine scale distribution of SST and satellite-derived phytoplankton niches (Lehahn et al. 2007; Rossi et al. 2008; d'Ovidio et al. 2010).

By combining the analysis of available near-real time satellite resources with derived Eulerian and Lagrangian diagnostics in an automated way, Petrenko et al. (2017) set up a new approach for real-time adaptive *fine scale* sampling strategy during the LATEX10 cruise in 2010. An automated algorithm, the Software Package for an Adaptive Satellite-based Sampling for Oceanographic cruises (SPASSO), was developed to provide on-board teams with daily maps of: near-real time satellite-derived surface currents, SST and Chl concentration and altimetry-derived Eulerian and Lagrangian diagnostics. This methodology filled the need for assessing in real-time a detailed description of the sampling area to opportunely study various biophysical processes such as the dynamic of an hyperbolic point and associated dispersion processes (LATEX10 cruise; Petrenko 2010), biogeochemical budgets associated with mesoscale phytoplankton bloom (OUTPACE cruise; Moutin and Bonnet 2015), natural iron fertilization in the Southern Ocean (KEOPS-II cruise; Queguiner 2011), or fine scale biophysical coupling (OSCAHR cruise; Doglioli 2015).

The new Surface Water and Ocean Topography (SWOT) satellite mission, launched in late 2022, offers a one of a kind opportunity to investigate the *fine scale* dynamics of the upper ocean, at

unprecedented horizontal and temporal resolutions, and to address the *fine scale* influence on the global energy budget in the ocean (d'Ovidio et al. 2019). Indeed during the calibration and validation (CalVal) period, from March to July 2023, the satellite recorded cloud-free SSH observations along both SWOT swaths (120 km wide) with a 1-day repeat: the 1-day orbit, or *fast-sampling* phase (Morrow et al. 2019). An international effort, conducted in the framework of the SWOT-Adopt-A-Crossover (AdAC) consortium, was carried out to coordinate *in situ* observations at orbit crossover points, hence visited twice a day during the fast-sampling phase. Endorsed by CLIVAR in 2019, this initiative encompasses more than 20 *in situ* experiments planned in a variety of ocean regions during the CalVal phase. The need to uniformly support all SWOT-AdAC cruises in their sampling strategies motivated the development of an updated version (v2.0) of the SPASSO software aiming to: 1) easily enable the code configuration for simultaneous multiple fields experiments during SWOT fast-sampling phase; 2) facilitate its autonomous use by a wide range of oceanographers; 3) develop new diagnostics designed to address innovative biophysical issues.

In the following we provide a complete description of the SPASSOv2.0 software architecture and functioning. Examples of SPASSO-generated maps are displayed and the computation of available Eulerian and Lagrangian diagnostics is detailed (Section 2). To illustrate the software capabilities and efficiency to guide future successful *fine scale* biophysical studies, we present several case studies of previous SPASSO-based *in situ* sampling experiments which occurred in various oceanic regions (Section 3).

2. Material and methods

a. Software architecture and philosophy

A key characteristic of the new SPASSOv2.0 framework is to provide a complete Python environment that encapsulates a set of functionalities to: 1) download ocean data; 2) perform dynamical analysis; 3) visualize and save ocean parameters. The tool is designed following modern scientific engineering software development and considering two main concepts:

(i) Ease of use: Software usage must be accessible to various oceanographers from different fields that are not always familiar with complex model computation. Therefore, a standard configuration

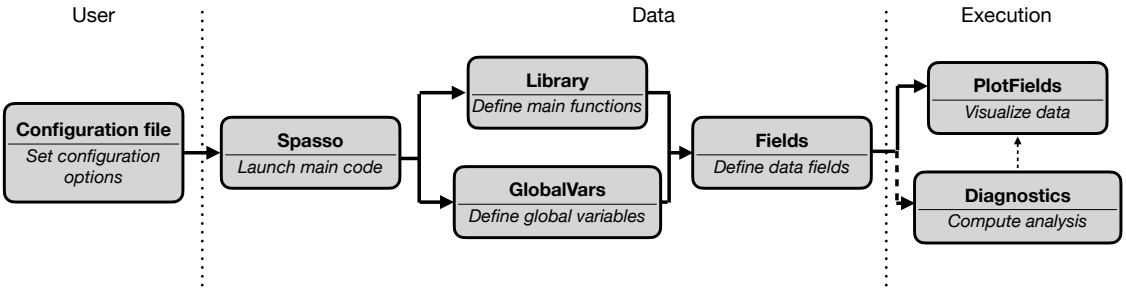

FIG. 1. Functionalities and structure of the SPASSOv2.0 algorithm.

of the software is openly accessible through Github (https://github.com/OceanCruises/SPASSO) and can be implemented by modifying a unique file controlling the algorithm main options.

(ii) Modularity and flexibility: The algorithm is designed to allow for the addition of various specialized sub-components (data, plotting options, outputs) to match different ocean sampling objectives without modifying the core code.

The main code (`Spasso.py`) first reads a text configuration file (`config_*.ini`) containing all the necessary options to run SPASSOv2.0 (Fig.1). In the configuration file, the user sets specific options related to his configuration such as: the cruise name and domain, the type of configuration (near-real time or delayed-time), the list of the desired satellite products and associated parameter limits, the list and parameter details for Eulerian and Lagrangian configuration and some output file options. The configuration file is the ONLY file the user needs to modify for a standard configuration of the code. After reading the configuration file, SPASSOv2.0 loads the necessary functions (`Library.py`) and global variables (`GlobalVars.py`) requested from the configuration file options. Then, the satellite data required by the user are downloaded and stored by `Fields.py`. A second layer is then in charge of plotting the downloaded data for visualization (`PlotFields.py`) and optionally computing some diagnostics for dynamical analysis (`Diagnostics.py`). The data used by SPASSOv2.0 are mainly satellite-derived physical and biogeochemical ocean variables (surface currents, SSH, SST, Sea Surface Salinity and surface Chl concentration) freely available, in near-real time, distributed by different platforms such as the European Copernicus marine data store (CMEMS). A novel option available in SPASSOv2.0 allows for the use of delayed-time available data to perform climatological and post-sampling analysis.

Figure 2 shows an example of three typical maps generated by SPASSOv2.0 configured to use SSH, surface currents, SST and Chl from CMEMS near-real-time products in the Indian sector of the Southern Ocean. These datasets provide some satellite-derived contextual information for spring 2011 (Queguiner 2011, KEOPS-II cruise). The satellite image analysis highlights the circulation of the major branch of the Antarctic Circumpolar Current, north of the Crozet Plateau, associated with the SubAntarctic Front (SAF) (Fig. 2a and b). For this specific example, we show the SAF position as detected by the local maxima of the SST gradient magnitude following a traditional gradient-based front identification method (see more detail in Wang et al. (2023) Supplementary Material). An intense phytoplankton bloom, constrained in cold waters to the south by the SAF, is visible on the chlorophyll-a image (Fig. 2c). The horizontal distribution of the bloom around the Crozet Plateau is structured by the surface currents measured by altimetry. The analysis of this coupling can be extended by computing some classical Eulerian and Lagrangian diagnostics (`Diagnostics.py`) provided by an embedded complementary software package coupled with SPASSOv2.0.

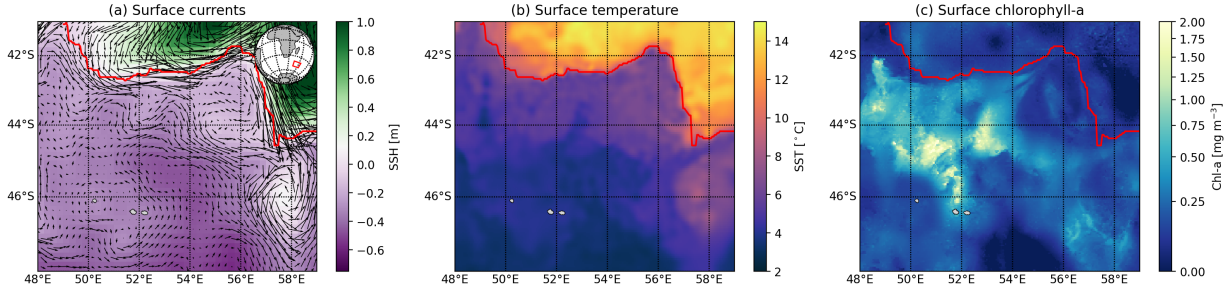

FIG. 2. Satellite-derived (a) Sea Surface Height and velocities (colorscale, m); (b) Sea Surface Temperature (colorscale, °C); (c) Surface Chlorophyll-a concentration (colorscale, mg.m^{-3}) for October 14^{th}, 2011. Red line shows the SubAntarctic Front (SAF) defined as the local maxima of satellite-derived SST gradient magnitude. Data were retrieved from the Copernicus Marine Data Store for the following products: (a) velocities and SSH: https://doi.org/10.48670/moi-00148; (b) SST: https://doi.org/10.48670/moi-00168; Chl-a: daily cmems_obs-oc_glo_bgc-plankton_my_l4-gapfree-multi-4km_P1D

b. Eulerian and Lagrangian analysis: LAMTA software

SPASSOv2.0 is coupled with a Python Lagrangian software (LAgrangian Manifolds Tracking Algorithm, LAMTA included in the `Diagnostics.py` file) that computes some Eulerian and Lagrangian diagnostics to provide statistics of the considered velocity field. Lagrangian diagnostics are derived from the trajectories of virtual particles analyzed to provide a complementary hydrodynamical description of the sampled region flow. Lagrangian ocean analysis are now widely used by the marine scientists community to track water masses, coherent structures, marine debris or biological dispersion (Van Sebille et al. 2018). LAMTA has been developed to advect virtual particles in horizontal 2-D time-evolving velocity fields and process the resulting trajectories to provide insights on the ocean circulation and dynamics (d'Ovidio et al. 2015). The Lagrangian diagnostics, including tracer advection, Lagrangian Coherent Structure (LCS) detection and water masses Lagrangian age, are provided as daily surface fields. These quantities are of particular interest for planning oceanographic sampling since they include history on the horizontal motion of seawater parcels. In the following, we describe the Eulerian diagnostics, the particle trajectory computation and the derived Lagrangian diagnostics computed by the LAMTA software.

Eulerian diagnostics:

The surface **kinetic energy (KE)** estimated from altimetry-derived geostrophic currents is often used to study the variability of surface ocean currents and eddies. We define KE at a given time as the total kinetic energy, including mean flow and eddy contributions. KE thus represents the amount of energy due to flow motion (Fig. 3a). It is expressed as the sum of the squared velocities (u, v), in $cm^2.s^{-2}$:

$$KE = u^2 + v^2 \tag{1}$$

The identification of ocean mesoscale eddies is particularly useful since they are believed to play significant roles in ocean heat and salt exchanges (Jayne and Marotzke 2002; Dong et al. 2014; Zhang et al. 2014) as well as on primary production, intermediate trophic levels and large predators (Falkowski et al. 1991; Cotté et al. 2007; Gaube et al. 2018; Della Penna and Gaube 2020). Different eddy detection methods have been developed and compared to identify mesoscale features (Souza et al. 2011). One of them is based on the **Okubo-Weiss parameter** (W) which

compares at a given point (i, j) the intensity of the strain (S) to the vorticity (ω) (i.e. the importance of deformation *versus* rotation in $days^{-2}$):

$$W_{i,j} = Sn_{i,j}^2 + Ss_{i,j}^2 - \omega_{i,j}^2 \tag{2}$$

where $Sn_{i,j}$ is the normal strain, $Ss_{i,j}$ is the shear strain and $\omega_{i,j}$ is the relative vorticity. These quantities are evaluated from the derivative of the daily surface geostrophic velocity fields (u, v) derived from altimetry:

$$Sn_{i,j} = \frac{\partial u}{\partial x}_{i,j} - \frac{\partial v}{\partial y}_{i,j}$$
$$Ss_{i,j} = \frac{\partial u}{\partial y}_{i,j} + \frac{\partial v}{\partial x}_{i,j}$$
$$\omega_{i,j} = \frac{\partial v}{\partial x}_{i,j} - \frac{\partial u}{\partial y}_{i,j}$$

Negative values of W identify regions of recirculation that can be associated with eddy cores, while positive W locate prevailing stretching areas (Fig. 3b). Isolines of W can be used to identify Eulerian eddy boundaries. However, since this diagnostic does not consider the temporal variability of the velocity field, it fails at representing the complex filamentous structures associated with eddy stirring. These *fine scale* characteristics of the flow can be more reliably assessed in a Lagrangian framework involving numerical particle trajectories computation.

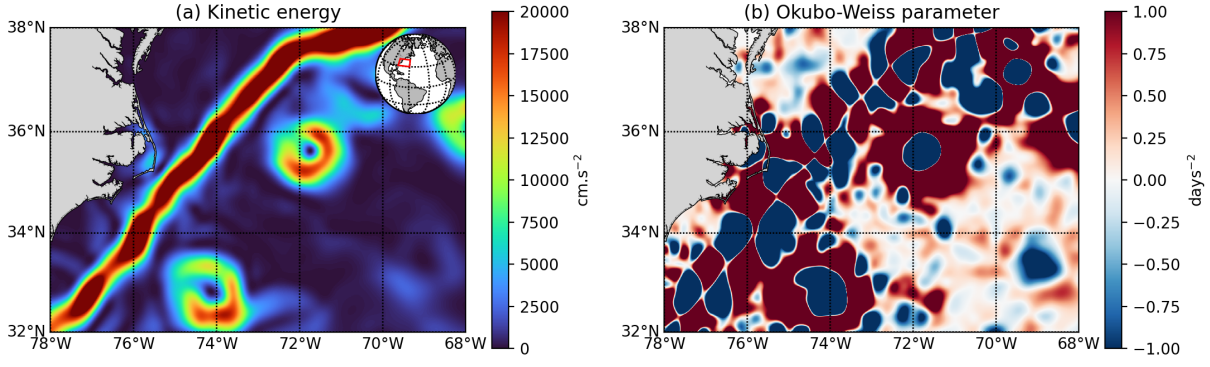

FIG. 3. (a) Kinetic energy (colorscale, $cm.s^{-2}$) and (b) Okubo-Weiss parameter (colorscale, $days^{-2}$) computed with satellite-derived geostrophic velocities from July 24^{th}, 2022 (https://doi.org/10.48670/moi-00148).

Off-line trajectory calculation:

Particle trajectories are computed off-line using horizontal 2-D velocity fields either stored from altimetry or Eulerian model outputs. Trajectories can be computed in a forward or backward in-time mode. Since water parcels history is traced back in SPASSOv2.0, LAMTA is set up by default in a backward mode.

Virtual particles can either be seeded from a list of locations (x, y) and times (t) provided by the user or can be initialized over a regular 2-D horizontal grid with a predefined resolution δ_s at a certain time t. The default seeding is over the entire domain and at the time of observation. A fine spatial seeding resolution (i.e. small δ_s) results in higher horizontal resolution Lagrangian diagnostics but also exponentially increases computing time. A trade-off between resolution and computing time must be considered when choosing δ_s, especially for large regions of interest.

Particle advection is then performed by (1) interpolating in space and time the gridded velocity field to each individual particle position; (2) integrating in time the trajectory. LAMTA's architecture allows users for coding their preferred methods for spatial interpolation and explicit time stepping. In the following we detail the default LAMTA set-up for a typical SPASSOv2.0 use. Each individual particle position $X(t)$ is updated by time-stepping the velocity at $X(t) = x$:

$$\mathbf{X}(t+\Delta t) = \mathbf{X}(t) + \int_t^{t+\Delta t} v(\mathbf{x}(\tau), \tau) d\tau \tag{3}$$

To accurately estimate the particle displacement, a fourth-order Runga-Kutta method is used for the integration of Eq.3: the interpolated velocity field is evaluated every 6 hours. Within grid cells, velocities are estimated using a linear 2-D interpolation. Once computed, the resulting trajectories are used to derive several Lagrangian diagnostics such as tracer advection, Lagrangian Coherent Structures and transit times.

Tracers advection:

Computed in non-divergent flows, Lagrangian tracer patches conserve mass and volume. Several Lagrangian tools have been developed to map volume transport pathways by attributing small amount of transport, conserved along the trajectories, to each virtual particle (Blanke and Raynaud

1997; Döös et al. 2017). Similarly, tracers' dispersion can be studied by attributing a portion of a tracer quantity assumed to be conserved for a given period equal to the virtual particle advection time.

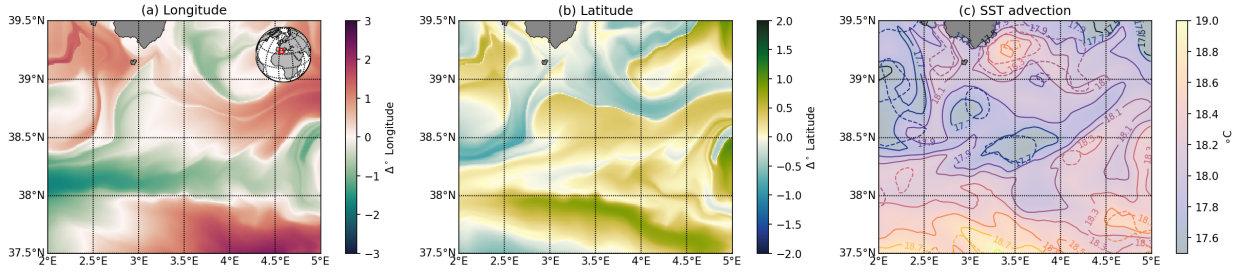

FIG. 4. (a) Longitude (left) and (b) latitude (right) advection computed from Lagrangian trajectories initiated on May 11, 2018 on a 0.01 degree grid and advected backward in time for 15 days using altimetry derived velocities (Mediterranean product from Copernicus Marine Data Store: https://doi.org/10.48670/moi-00141). (c) SST advected (shaded colormap and plain contours) backward for 3 days from May 11, 2018. The dashed contours show the SST field on May 11, 2018 before advection (SST product from Copernicus Marine Data Store: METOFFICE-GLO-SST-L4-REP-OBS-SST).

Another way to study content advection is to map the difference between the tracer value at the initial and final position of the virtual particle. Tracer/content values are defined from the satellite-derived value identified at the time and location of the particle (Barceló-Llull et al. 2021). In SPASSOv2.0 tracer advection maps (SST, SSS or chlorophyll-a) can be computed with this method. A default advection time of 3 days is considered for these non-conservative tracers: Figure 4c shows a map of temperature advection from a satellite derived SST field. Advection maps of longitude or latitude can also help identifying water masses origin. This diagnostic measures the difference in longitudes (or latitudes) between each initial and final particle position. A typical value of 12 to 15 days for particle advection is recommended for these diagnostics to assume that water masses conserved the initial characteristics they had at their origin. Figure 4a,b show an example of longitude and latitude advection maps computed south of the Balearic Islands in the Mediterranean Sea. Green patches identify regions where water parcels were located anywhere east of the grid cell 15 days before; whereas red areas indicate a western origin. Similar conclusions can be inferred from the latitude advection map in the North-South direction: blue (yellow) patches reveal a northern (southern) origin respectively. Strong gradients of these advections can also

be used to detect frontal areas between potentially different water masses moving in opposite directions.

Lagrangian Coherent Structure detection:

Coherent structures such as eddies, jets and fronts are ubiquitous features in the ocean that drive the distribution of ocean tracers and impact ocean biogeochemistry (Smith et al. 2016; Mahadevan 2016; Zhang et al. 2019). The Lagrangian Coherent Structures (LCS) theory relies on the detection of distinct coherent regions, separated by clear boundaries, based on Lagrangian trajectory analysis. One empirical diagnostic of LCSs is the Finite Time Lyapunov Exponent (FTLE) which identifies attracting and repelling material structures (Lapeyre 2002). FTLE (λ) computed from a backward in time integration measures the exponential rate of separation between water parcels initially at a close distance from one another, and is defined as (Eq. 4):

$$\lambda = \frac{1}{2}\frac{log(\frac{d_f}{d_i})}{T} \tag{4}$$

with d_f the final particle separation (distance), d_i the initial particle separation (distance) and T the integration time (i.e. number of days of integration).

The backward FTLE diagnostic identifies attracting LCSs along which water parcels tend to accumulate due to horizontal stirring even if they were originally located at large distance apart. Because of that, the ridges (i.e. local maxima) of Lyapunov exponents, computed from altimetry data, can be used to identify stirring regions where water masses are relatively quickely elongated. Figure 5a shows FTLEs associated with the highly energetic Gulf Stream and related rings: the current and eddy boundaries intensely stir the water masses, as revealed by the FTLEs filaments. These features can thus be used to indentify frontal regions acting like barriers to the flow. On the contrary, regions of low or null FTLEs, highlighted in black on Figure 5a emphasize zones with low stirring effect. Several studies have already shown the correlation between the detected structures from Lyapunov exponents and the distribution of tracer gradients (Lehahn et al. 2007; d'Ovidio et al. 2009; Rousselet et al. 2018), or the location of biological niches (d'Ovidio et al. 2010; De Monte et al. 2012; Della Penna et al. 2017). These previous studies computed the so-called Finite Size Lyapunov Exponent (FSLE): the lyapunov exponent is calculated only for particle pairs

when they reach a d_f equal or greater than a predefined distance (or size, as its name suggests). The FSLE computation can take an infinite time if we wait for all particles to reach the final distance. The FTLE theory instead computes Lyapunov exponents for all particles advected for a finite time, regardless of their final separation. In this version of LAMTA, we chose to compute FTLE rather than FSLE because the FSLE concept particle integration needs to be bounded in time anyway.

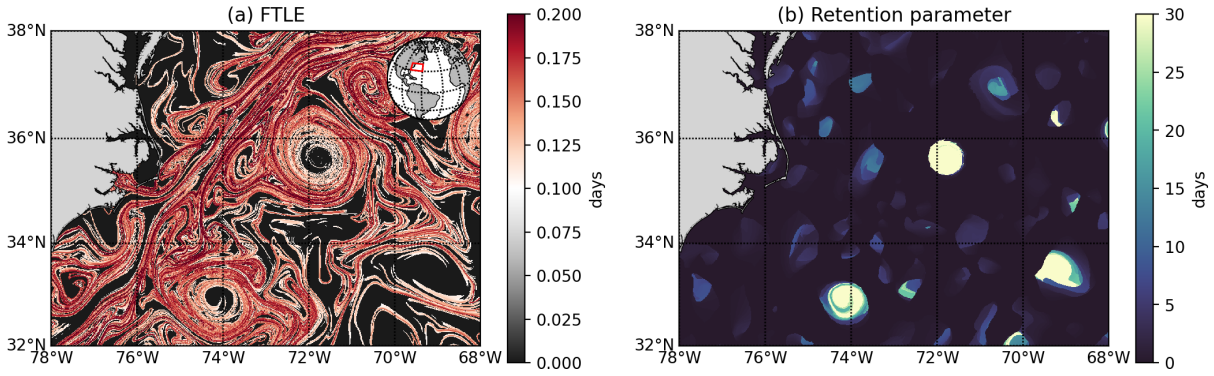

FIG. 5. (a) Finite-Time Lyapunov exponents (colorscale in days^{-1}) (FTLE). (b) Retention parameter (colorscale, days) computed from 30 days backward trajectories initiated on a 0.01 degree grid on July 22nd, 2022 using altimetry derived velocities (https://doi.org/10.48670/moi-00148).

Other significant coherent structures commonly tracked are oceanic mesoscale eddies, due their ability to trap and transport water masses and their biotic and abiotic contents. If the Lyapunov exponents can detect enclosed filaments associated with some eddy cores, they fail at estimating the trapping nature of eddies. One crucial information to understand some of the biological dynamics related to ocean eddies is in fact the timescale of eddy trapping. d'Ovidio et al. (2013) have defined the Retention Parameter (RP) that evaluates the time a water parcel recirculates within an eddy. Unlike traditional eddy tracking algorithm usually based on the detection of sea level anomaly, vorticity or streamlines closed contour (Haller 2015; Le Vu et al. 2018; Laxenaire et al. 2018), the RP calculation is an hybrid Eulerian-Lagrangian method based on the evaluation of the OW parameter along backward Lagrangian trajectories. As long as the OW parameter remains successively negative, the particle is considered trapped in an eddy core. Once the OW parameter changes sign (i.e. becomes positive), the particle is treated as out of the eddy. Therefore the RP is

defined as the time of persistence of a negative OW value. Compared to the Eulerian OW parameter diagnostic, the RP identifies only structures able to trap water in their core (Fig. 3c).

Lythogenic water masses age and transit:

Nutrient enrichment of water masses by contact with a topographic feature such as coasts, shelf

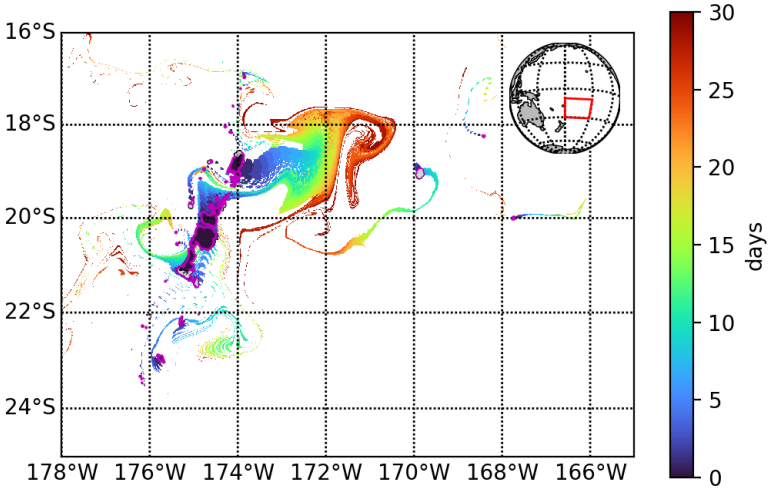

FIG. 6. Water parcels lythogenic age (colorscale in days) since they were in contact with isobath z = -200 m marked by magenta contours. Lagrangian trajectories were initiated on a 0.01 degree grid resolution and computed from 30 days backward advection starting on March 8^{th}, 2015 using using altimetry derived velocities (https://doi.org/10.48670/moi-00148).

breaks, sea mounts or hydrothermal vents is a crucial physical process leading to biological enhancement. A Lagrangian approach developed by d'Ovidio et al. (2015) considers the time since the last contact with an isobath ('water age') chosen according to the topographic element depth.Technically, 2-D backward-in-time trajectories are checked for crossing any area where ocean depths are shallower than the selected isobath anytime during the time integration. If a trajectory never reaches a region above the chosen isobath then it is discarded from the water age calculation. The time taken by the particle to reach the isobath is assigned to the initial particle grid cell. This means the water parcel located in this area was in contact with the topographic feature, defined by the isobath threshold, X days ago. Theoretically this lythogenic water age diagnostic allows for the identification of water patches potentially nutrient-enriched by contact with coastal or deep sediments. Figure 6 shows an example of a water patch previously in contact with the Tonga

islands in the southwest Pacific: the waters located at 172°W and 18°S were near the Tonga island coasts 20 days prior 8 March 2015. This diagnostic has been previously matched with the surface distribution of satellite-derived Chl patches and surface drifters (d'Ovidio et al. 2015; Sanial et al. 2014, 2015; Sergi et al. 2020; Chabert et al. 2021).

3. Biophysical applications

In its early stages, SPASSO was used to specifically track *fine scale* processes and features such as the evolution of the dynamics associated with persistent mesoscale eddies (LATEX cruises, Petrenko et al. 2017), or to monitor the impact of horizontal advection in regulating the salinity maximum within the subtropical gyre (STRASSE cruise, Reverdin et al. 2015). However it rapidly proved to be quite useful for biophysical applications of growing interests lately. This section reviews how SPASSO can help design sampling strategies to elucidate biophysical processes at *fine scales*. We selected the following examples as they span a large variety of oceans and seas (Atlantic, Pacific, Southern Ocean and Mediterranean Sea) as well as physically and biologically contrasted environments: productive boundary current, open ocean oligotrophic areas or High-Nutrient, Low-Chlorophyll (HNLC) region.

a. Natural ocean fertilization effect on phytoplankton blooms

Phytoplankton blooms are episodic and rapid population increase events often driven by an unusual supply of limiting nutrients. In the case of seasonal blooms, the simultaneous availability of light energy along with nutrient resources (or a rapid decrease in grazing pressure) is also required for photosynthesis and phytoplankton growth. Submesoscale horizontal and vertical transport is one among the physical processes (restratification, solar forcing, surface heating) participating in enhancing phytoplankton blooms whether they occur in coastal, oligotrophic or HNLC regions (Mahadevan 2016; Lévy et al. 2018).

The main goal of the KEOPS-2 campaign was to study the potential influence of natural iron fertilization on phytoplankton blooms off the Crozet Plateau around the Kerguelen islands in the Southern Ocean (Queguiner 2011). SPASSO outputs were perfectly suited to identify such a bloom from space and plan *in situ* sampling. SPASSO maps of surface Chl were used to locate the bloom and displayed a surface patch expanding from the Crozet Islands (~46°S-52°E) further north until

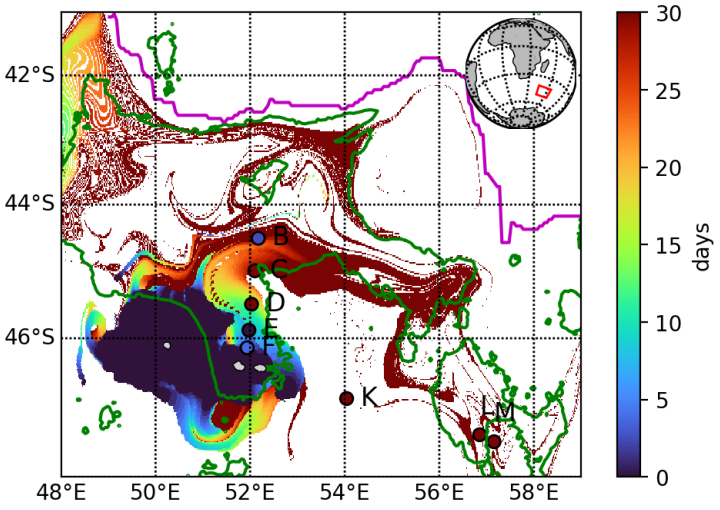

FIG. 7. Reproducing Sanial et al. (2014) results: Water ages (colorscale, days) since lying above the 2000 m isobath (isobath limit is shown by the limit of initial age = 0 days). The Lagrangian trajectories are advected from October 14th, 2011 for a maximum of 80 days using the satellite-derived velocities (https://doi.org/10.48670/moi-00148). The magenta line marks the SAF front identified by the maximum SST gradient (Fig. 2). The green line contours satellite chlorophyll-a concentration above 0.25 mg.m^{-3}. Colored dots (same color scale, days) show the apparent radium ages of surface waters derived from ^{224}Ra/^{228}Ra ratios (more details in Sanial et al. (2014)).

restricted by the SubAntarctic Front (SAF, Fig. 2c). The bloom extension and SAF position are also shown by the green and magenta lines respectively on Figure 7. The water mass ages were also estimated from the 2000 m isobath to mimic the potential deep-ocean iron fertilization. The water mass age patch distribution matches the distribution of significantly high values of surface Chl (Fig. 2c and green contour on Fig. 7). SPASSO output analysis thus suggests that the seasonal phytoplankton bloom has been triggered by a deep-water iron enrichment: the relatively good overlay between both independent estimates of Chl-a concentration and Lagrangian lythogenic water mass age indicates a potential influence of physical processes in driving and shaping the bloom. In order to validate the lythogenic water mass age diagnostic, Sanial et al. (2014) estimated the age of surface waters from radium isotopic ratios. The colored dots on Figure 7 show an increase in water age with the distance from the Crozet Islands. However the farthest station (B) is characterized by relatively younger waters (~8 days old) indicating a more recent interaction with the shelf sediments than stations (C,D) located closer to the islands. This pattern is probably due to

a small-scale circulation stirring a tongue of young waters in contact with the northern boundary of the Plateau further east. This tongue is actually visible on the lythogenic water age at around 45°S-51°E but does not extend east enough probably because of the poor accuracy (at that time) of altimetry-derived geostrophic currents near the coast.

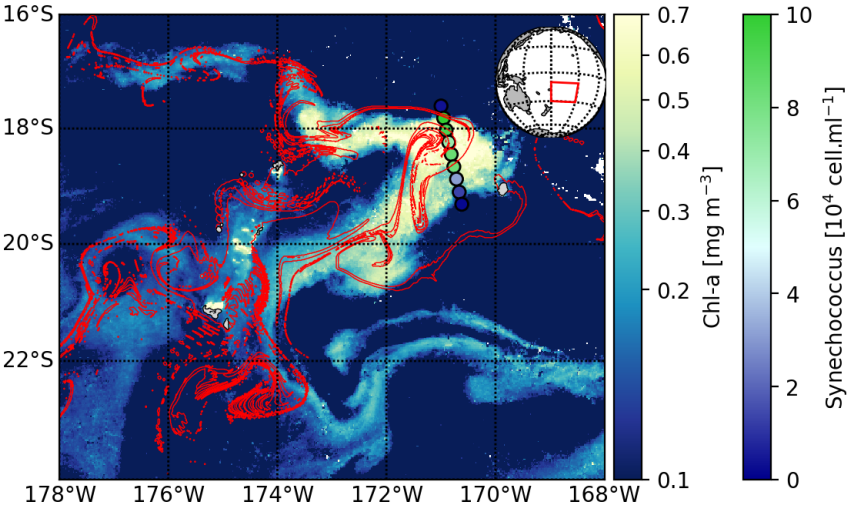

FIG. 8. Satellite-derived surface chlorophyll-a concentration (colorscale in mg m−3) on March 8th, 2015 extracted from de Verneil et al. (2017) and Rousselet et al. (2018) results. Contours of "enriched" water patches derived from water age diagnostic (Fig 6) are shown in red.

Another phytoplankton bloom has been sampled in the ultra-oligotrophic South Pacific ocean during the OUTPACE cruise (Moutin et al. 2017). The main objectives of OUTPACE were to characterize the distribution of biogeochemical elements and biological diversity along an oligotrophic gradient (i.e. depleted nutrient environments). Halfway through the cruise, SPASSO images revealed a spectacular unusual phytoplankton bloom marked by relatively high Chl concentration in the vicinity of Tonga Islands (Fig. 8). *In situ* high-resolution biological sampling confirmed the location of the bloom (Rousselet et al. 2018) as shown by the *Synechococcus* abundances on Figure 8. The patch of lythogenic water ages (red contours) initiated at 200 m (i.e. around the Tonga Islands) matched the surface distribution of satellite-derived Chl suggesting the bloom could be induced by a near-surface coastal nutrient enrichment. This hypothesis have then been confirmed by further Lagrangian analysis and the mechanism in place has been defined as a delayed island

mass effect (IME) where mesoscale circulation create a hotspot of productivity by transporting nutrient enriched waters (de Verneil et al. 2017; Messié et al. 2020).

b. Eddy influence on primary production

Gulf Stream rings are certainly the most studied eddies in ocean research history since the pioneer observations in the 1970's (Richardson et al. 1978). Although several studies already fully describe the formation, evolution and biological implications of warm-core and cold-core Gulf Stream rings, a subtancial knowledge can be derived by sampling a Gulf Stream eddy with high frequency multiplatform sampling technologies and methods. The FIGURE-CARING cruise (Benavides and Carracedo 2022) was guided by SPASSO to a large mesoscale eddy with a non-negligible Chl signature, while heading towards the North Atlantic to cross-sample the Gulf Stream (Fig. 9).

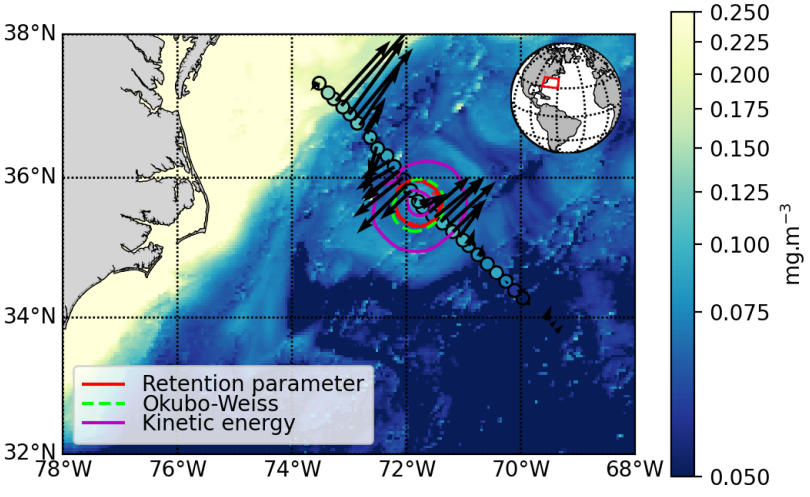

FIG. 9. Satellite-derived chl concentration (color scale, mg.m^{-3}) for 24 July 2022 (product from Copernicus Marine Data Store: cmems_obs-oc_glo_bgc-plankton_myint_l4-gapfree-multi-4km_P1D). Contours of retention parameter (25 days) in red, Okubo-Weiss parameter (-1 days^{-2}) in dashed green and kinetic energy (7000 cm.s^{-2}) in magenta. Arrows show surface currents from ADCP (first level at 27 m). Colored dots show surface chl concentration (color scale, mg.m^{-3}) from underway sea water system every 3 minutes for visualization purposes.

A high resolution biophysical cross-eddy sampling was planned based on SPASSO diagnostics information. The core and eddy center were accurately determined using several Eulerian and Lagrangian-based diagnostics (KE, OW and FSLE) as revealed by the surface current measured by the hull-mounted vessel ADCP (Fig. 9). High-frequency sampling (every 5 seconds) of the surface Chl concentration displays a similar gradient of surface Chl as the one detected by satellite. High-resolution measurements of N_2 fixation rates conducted across the eddy revealed substantially higher eddy-induced rates, associated with consistent detection of Trichodesmium cells, than previously reported in the western North Atlantic (Hoerstmann et al. 2023). Overall, these feature-oriented observations demonstrate that eddies contribute significantly to diazotrophy and thus to reactive nitrogen input in the western North Atlantic.

c. Fronts and biological niches

The few observations focusing on frontogenesis influence over phytoplankton diversity usually took place in persistent and intense fronts generated by energetic boundary currents or coastal upwellings (Ribalet et al. 2010; Clayton et al. 2017). However, most of the global ocean is characterized by weakly energetic and short-lived features. One of the main objectives of the PROTEVSMED-SWOT cruise was to observe (sub)mesoscale circulation and associated ageostrophic dynamics in the moderately energetic open Mediterranean Sea (Dumas 2018). Based on SPASSO analysis, simultaneous physical and biological high-frequency measurements were performed, south of the Balearic Islands, in a potential frontal area marked by a surface Chl gradient (Tzortzis et al. 2021). The analysis of FTLE distribution and water mass origins also suggested the presence of a front separating biogeochemically contrasted areas.

Figure 10 shows a global water mass origin map produced during post-processing by combining both longitude and latitude advection maps from Figure 4. Each color map refers to a relative orientation on a compass rose (SouthWest, NorthWest, SouthEast and NorthEast) and follows the wind direction formalism (i.e. coming from). Figure 10 thus highlights that most of the waters in the 38.5°N-39°N band are globally coming from the west whereas waters in the 38.5°N-38°N travel from East to West. This contrast in water mass origins is confirmed by the hydrological characteristics measured at high-frequency with a CTD mounted on a towed vehicle (see Tzortzis et al. (2021) for more details). For example the salinity dramatically changes at the boundary of the

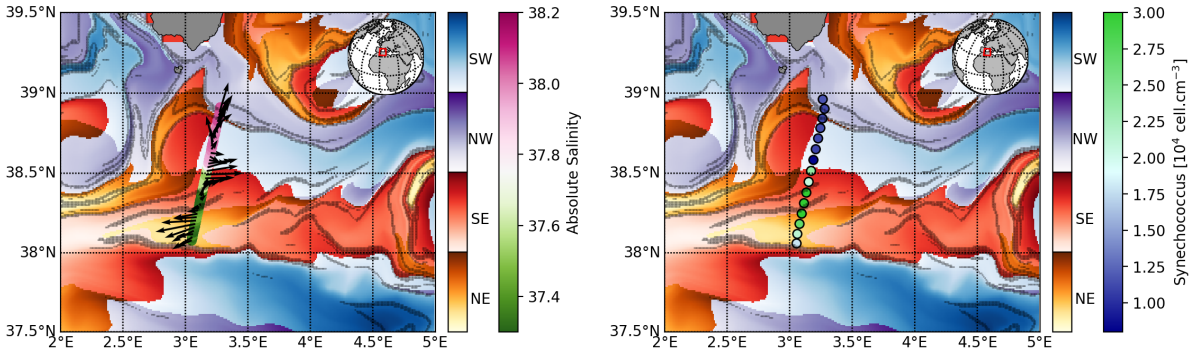

FIG. 10. Water parcels origin computed from longitude and latitude advections shown in Figure 4. The colorscale indicate geographical origin direction from the grid cell position (SW: SouthWest; NW: NorthWest; SE: SouthEast; NE: NorthEast). Black arrows show the current velocities measured by a vessel-mounted ADCP on May 11th, 2018 at 25 m depth. Near-surface absolute salinity measured with a SeaSoar vehicle along the cross-front transect is also shown with the green to pink colorscale and the Synechococus concentration with the blue to green colorscale (more details about *in situ* data acquisition and treatment in Tzortzis et al. (2021)).

two different water masses: northern saltier waters travel east whereas southern cooler waters flow west. The Lagrangian-based water mass origins and directions are coherent with surface currents estimated from the hull-mounted ADCP. A FTLE-derived front also matches with the change in direction from surface currents. The distribution of phytoplankton abundances (*Synechococcus* on Figure 10) shows an across front contrast in phytoplankton diversity: some groups are dominant on one or the other side of the front thus creating biological niches. SPASSO analysis allowed for sampling a contrasted front whose 3D fine-scale biophysical description and history was completed by post-cruise investigations (see Tzortzis et al. 2021, 2023).

4. Conclusions

In this paper, we have introduced the new user-friendly Python version of the SPASSO software and detailed the Eulerian and Lagrangian diagnostics available for near-real time ocean analysis. We have also documented potential biophysical applications and assess the current code accuracy based on previous scientific experiments that were conducted using previous less well-developped SPASSO version. This represent a benchmark for future usages especially in the context of the new altimetric SWOT mission and field experiments conducted in the framework of the SWOT-AdAC

consortium (`https://www.swot-adac.org`). Future evaluation of SPASSO-based strategies will arise from the analysis of the *in situ* SWOT-AdAC sampling experiments that will provide a large overview of the *fine scales* in diverse oceans and regions (coastal vs. open ocean, eutrophic vs. oligotrophic, highly vs. weakly energetic). Additionally, future versions of SPASSO will benefit from the new high-resolution SWOT products, when available, enabling for the first time very *fine scale* features detection.

Acknowledgments. SPASSOv2.0 development was supported and funded by CNES (Centre National d'Études Spatiales), LOCEAN (Laboratoire d'Océanographie et du Climat: Expérimentations et Approches Numériques), Sorbonne University and MIO (Mediterranean Institute of Oceanography), Aix-Marseille University. SPASSO (https://spasso.mio.osupytheas.fr) is also operated with the support of the SIP (Service Informatique de Pythéas) and in particular C. Yohia, J. Lecubin. D. Zevaco and C. Blanpain (Institut Pythéas, Marseille, France).

Code availability. The code for SPASSO is licensed under the MIT licence and version 2.0 is available through GitHub at https://github.com/OceanCruises/SPASSO/.

References

Abdalla, S., and Coauthors, 2021: Altimetry for the future: Building on 25 years of progress. *Advances in Space Research*, **68 (2)**, 319–363.

Barceló-Llull, B., K. Drushka, and P. Gaube, 2021: Lagrangian Reconstruction to Extract Small-Scale Salinity Variability From SMAP Observations. *Journal of Geophysical Research: Oceans*, **126 (3)**, e2020JC016 477.

Benavides, M., and L. Carracedo, 2022: FIGURE-CARING cruise. *RV Atlantic Explorer*, https://doi.org/10.17600/18002940.

Biggs, D. C., 1992: Nutrients, plankton, and productivity in a warm-core ring in the western Gulf of Mexico. *Journal of Geophysical Research: Oceans*, **97 (C2)**, 2143–2154.

Blanke, B., and S. Raynaud, 1997: Kinematics of the Pacific equatorial undercurrent: An Eulerian and Lagrangian approach from GCM results. *Journal of Physical Oceanography*, **27 (6)**, 1038–1053.

Brekhovskikh, L., K. Fedorov, L. Fomin, M. Koshlyakov, and A. Yampolsky, 1971: Large-scale multi-buoy experiment in the tropical Atlantic. *Deep Sea Research and Oceanographic Abstracts*, Elsevier, Vol. 18, 1189–1206.

Chabert, P., F. d'Ovidio, V. Echevin, M. Stukel, and M. D. Ohman, 2021: Cross-shore flow and implications for Carbon Export in the California Current Ecosystem: a Lagrangian analysis. *Journal of Geophysical Research: Oceans*, **126 (2)**, e2020JC016 611.

Clayton, S., Y.-C. Lin, M. J. Follows, and A. Z. Worden, 2017: Co-existence of distinct Ostreococcus ecotypes at an oceanic front. *Limnology and Oceanography*, **62 (1)**, 75–88.

Cotté, C., Y.-H. Park, C. Guinet, and C.-A. Bost, 2007: Movements of foraging king penguins through marine mesoscale eddies. *Proceedings of the Royal Society B: Biological Sciences*, **274 (1624)**, 2385–2391.

De Monte, S., C. Cotté, F. d'Ovidio, M. Lévy, M. Le Corre, and H. Weimerskirch, 2012: Frigatebird behaviour at the ocean–atmosphere interface: integrating animal behaviour with multi-satellite data. *Journal of the Royal Society Interface*, **9 (77)**, 3351–3358.

de Verneil, A., L. Rousselet, A. M. Doglioli, A. A. Petrenko, and T. Moutin, 2017: The fate of a southwest pacific bloom: gauging the impact of submesoscale vs. mesoscale circulation on biological gradients in the subtropics. *Biogeosciences*, **14 (14)**, 3471–3486.

Della Penna, A., and P. Gaube, 2020: Mesoscale eddies structure mesopelagic communities. *Frontiers in Marine Science*, **7**, 454.

Della Penna, A., P. Koubbi, C. Cotté, C. Bon, C.-A. Bost, and F. d'Ovidio, 2017: Lagrangian analysis of multi-satellite data in support of open ocean Marine Protected Area design. *Deep Sea Research Part II: Topical Studies in Oceanography*, **140**, 212–221.

Doglioli, A., 2015: OSCAHR cruise. *RV Téthys II*, https://doi.org/10.17600/15008800.

Dong, C., J. C. McWilliams, Y. Liu, and D. Chen, 2014: Global heat and salt transports by eddy movement. *Nature communications*, **5 (1)**, 3294.

Döös, K., B. Jönsson, and J. Kjellsson, 2017: Evaluation of oceanic and atmospheric trajectory schemes in the TRACMASS trajectory model v6. 0. *Geoscientific Model Development*, **10 (4)**, 1733–1749.

d'Ovidio, F., and Coauthors, 2015: The biogeochemical structuring role of horizontal stirring: Lagrangian perspectives on iron delivery downstream of the Kerguelen Plateau. *Biogeosciences*, **12 (19)**, 5567–5581.

Dumas, F., 2018: PROTEVSMED-SWOT cruise. *RV Beautemps-Beaupré*, https://doi.org/10.17183/protevsmed_swot_2018_leg1.

d'Ovidio, F., S. De Monte, S. Alvain, Y. Dandonneau, and M. Lévy, 2010: Fluid dynamical niches of phytoplankton types. *Proceedings of the National Academy of Sciences*, **107 (43)**, 18 366–18 370.

d'Ovidio, F., S. De Monte, A. Della Penna, C. Cotté, and C. Guinet, 2013: Ecological implications of eddy retention in the open ocean: a Lagrangian approach. *Journal of Physics A: Mathematical and Theoretical*, **46 (25)**, 254 023.

d'Ovidio, F., J. Isern-Fontanet, C. López, E. Hernández-García, and E. García-Ladona, 2009: Comparison between Eulerian diagnostics and finite-size Lyapunov exponents computed from altimetry in the Algerian basin. *Deep Sea Research Part I: Oceanographic Research Papers*, **56 (1)**, 15–31.

d'Ovidio, F., and Coauthors, 2019: Frontiers in fine-scale in situ studies: Opportunities during the swot fast sampling phase. *Frontiers in Marine Science*, **6**, 168.

Falkowski, P. G., D. Ziemann, Z. Kolber, and P. K. Bienfang, 1991: Role of eddy pumping in enhancing primary production in the ocean. *Nature*, **352 (6330)**, 55–58.

Gaube, P., C. D. Braun, G. L. Lawson, D. J. McGillicuddy Jr, A. D. Penna, G. B. Skomal, C. Fischer, and S. R. Thorrold, 2018: Mesoscale eddies influence the movements of mature female white sharks in the Gulf Stream and Sargasso Sea. *Scientific reports*, **8 (1)**, 7363.

Gill, A., J. Green, and A. Simmons, 1974: Energy partition in the large-scale ocean circulation and the production of mid-ocean eddies. *Deep sea research and oceanographic abstracts*, Elsevier, Vol. 21, 499–528.

Gower, J., K. Denman, and R. Holyer, 1980: Phytoplankton patchiness indicates the fluctuation spectrum of mesoscale oceanic structure. *Nature*, **288 (5787)**, 157–159.

Group, M., and Coauthors, 1978: The mid-ocean dynamics experiment. *Deep Sea Research*, **25 (10)**, 859–910.

Haller, G., 2015: Lagrangian coherent structures. *Annual review of fluid mechanics*, **47**, 137–162.

Hoerstmann, C., and Coauthors, 2023: Diazotroph connectomics in Gulf Stream eddies supports N2 fixation in the North Atlantic.

Jayne, S. R., and J. Marotzke, 2002: The oceanic eddy heat transport. *Journal of Physical Oceanography*, **32 (12)**, 3328–3345.

Kavanaugh, M. T., M. J. Oliver, F. P. Chavez, R. M. Letelier, F. E. Muller-Karger, and S. C. Doney, 2016: Seascapes as a new vernacular for pelagic ocean monitoring, management and conservation. *ICES Journal of Marine Science*, **73 (7)**, 1839–1850.

Lapeyre, G., 2002: Characterization of finite-time Lyapunov exponents and vectors in two-dimensional turbulence. *Chaos: An Interdisciplinary Journal of Nonlinear Science*, **12 (3)**, 688–698.

Laxenaire, R., S. Speich, B. Blanke, A. Chaigneau, C. Pegliasco, and A. Stegner, 2018: Anticyclonic eddies connecting the western boundaries of Indian and Atlantic Oceans. *Journal of Geophysical Research: Oceans*, **123 (11)**, 7651–7677.

Le Vu, B., A. Stegner, and T. Arsouze, 2018: Angular momentum eddy detection and tracking algorithm (AMEDA) and its application to coastal eddy formation. *Journal of Atmospheric and Oceanic Technology*, **35 (4)**, 739–762.

Lehahn, Y., F. d'Ovidio, M. Lévy, and E. Heifetz, 2007: Stirring of the northeast Atlantic spring bloom: A Lagrangian analysis based on multisatellite data. *Journal of Geophysical Research: Oceans*, **112 (C8)**.

Lévy, M., R. Ferrari, P. J. Franks, A. P. Martin, and P. Rivière, 2012: Bringing physics to life at the submesoscale. *Geophysical Research Letters*, **39 (14)**.

Lévy, M., P. J. Franks, and K. S. Smith, 2018: The role of submesoscale currents in structuring marine ecosystems. *Nature communications*, **9 (1)**, 4758.

Mahadevan, A., 2016: The impact of submesoscale physics on primary productivity of plankton. *Annual review of marine science*, **8**, 161–184.

Mahadevan, A., and J. Campbell, 2002: Biogeochemical patchiness at the sea surface. *Geophysical Research Letters*, **29 (19)**, 32–1.

McClain, C. R., 2009: A decade of satellite ocean color observations. *Annual Review of Marine Science*, **1**, 19–42.

McGillicuddy Jr, D. J., 2016: Mechanisms of physical-biological-biogeochemical interaction at the oceanic mesoscale. *Annual Review of Marine Science*, **8**, 125–159.

McWilliams, J., and Coauthors, 1983: The local dynamics of eddies in the western North Atlantic. *Eddies in marine science*, Springer, 92–113.

McWilliams, J. C., 2006: *Fundamentals of geophysical fluid dynamics*. Cambridge University Press.

Messié, M., A. Petrenko, A. M. Doglioli, C. Aldebert, E. Martinez, G. Koenig, S. Bonnet, and T. Moutin, 2020: The delayed island mass effect: How islands can remotely trigger blooms in the oligotrophic ocean. *Geophysical Research Letters*, **47 (2)**, e2019GL085 282.

Millot, C., M. Benzohra, and I. Taupier-Letage, 1997: Circulation off Algeria inferred from the Mediprod-5 current meters. *Deep Sea Research Part I: Oceanographic Research Papers*, **44 (9-10)**, 1467–1495.

Morrow, R., and Coauthors, 2019: Global observations of fine-scale ocean surface topography with the surface water and ocean topography (SWOT) mission. *Frontiers in Marine Science*, **6**, 232.

Moutin, M., and S. Bonnet, 2015: OUTPACE cruise. *RV L'Atalante*, https://doi.org/10.17600/15000900.

Moutin, T., A. M. Doglioli, A. De Verneil, and S. Bonnet, 2017: Preface: The Oligotrophy to the UlTra-oligotrophy PACific Experiment (OUTPACE cruise, 18 February to 3 April 2015). *Biogeosciences*, **14 (13)**, 3207–3220.

Okubo, A., 1970: Horizontal dispersion of floatable particles in the vicinity of velocity singularities such as convergences. *Deep sea research and oceanographic abstracts*, Elsevier, Vol. 17, 445–454.

Peláez, J., and J. A. McGowan, 1986: Phytoplankton pigment patterns in the California Current as determined by satellite 1. *Limnology and Oceanography*, **31 (5)**, 927–950.

Petrenko, A. A., 2010: LATEX10 cruise. *RV Téthys II*, https://doi.org/10.17600/10450150.

Petrenko, A. A., A. M. Doglioli, F. Nencioli, M. Kersalé, Z. Hu, and F. d'Ovidio, 2017: A review of the LATEX project: mesoscale to submesoscale processes in a coastal environment. *Ocean Dynamics*, **67**, 513–533.

Queguiner, B., 2011: MD 188 / KEOPS 2 cruise. *RV Marion Dufresne*, https://doi.org/10.17600/11200050.

Reverdin, G., and Coauthors, 2015: Surface Salinity in the North Atlantic subtropical gyre: During the STRASSE/SPURS Summer 2012 Cruise. *Oceanography*, **28 (1)**, 114–123.

Ribalet, F., and Coauthors, 2010: Unveiling a phytoplankton hotspot at a narrow boundary between coastal and offshore waters. *Proceedings of the National Academy of Sciences*, **107 (38)**, 16 571–16 576.

Richardson, P. L., R. Cheney, and L. Worthington, 1978: A census of Gulf Stream rings, spring 1975. *Journal of Geophysical Research: Oceans*, **83 (C12)**, 6136–6144.

Ring Group, t., 1981: Gulf Stream cold-core rings: Their physics, chemistry, and biology. *Science*, **212 (4499)**, 1091–1100.

Rossi, V., C. López, J. Sudre, E. Hernández-García, and V. Garçon, 2008: Comparative study of mixing and biological activity of the Benguela and Canary upwelling systems. *Geophysical Research Letters*, **35 (11)**.

Rousselet, L., A. de Verneil, A. M. Doglioli, A. A. Petrenko, S. Duhamel, C. Maes, and B. Blanke, 2018: Large-to submesoscale surface circulation and its implications on biogeochemical/biological horizontal distributions during the OUTPACE cruise (southwest Pacific). *Biogeosciences*, **15 (8)**, 2411–2431.

Sanial, V., P. Van Beek, B. Lansard, F. d'Ovidio, E. Kestenare, M. Souhaut, M. Zhou, and S. Blain, 2014: Study of the phytoplankton plume dynamics off the Crozet Islands (Southern Ocean): A geochemical-physical coupled approach. *Journal of Geophysical Research: Oceans*, **119 (4)**, 2227–2237.

Sanial, V., P. van Beek, B. Lansard, M. Souhaut, É. Kestenare, F. d'Ovidio, M. Zhou, and S. Blain, 2015: Use of Ra isotopes to deduce rapid transfer of sediment-derived inputs off Kerguelen. *Biogeosciences*, **12 (5)**, 1415–1430.

Sergi, S., A. Baudena, C. Cotté, M. Ardyna, S. Blain, and F. d'Ovidio, 2020: Interaction of the Antarctic Circumpolar Current With seamounts fuels moderate blooms but vast foraging grounds for multiple marine predators. *Frontiers in Marine Science*, **7**, 416.

Smith, K. M., P. E. Hamlington, and B. Fox-Kemper, 2016: Effects of submesoscale turbulence on ocean tracers. *Journal of Geophysical Research: Oceans*, **121 (1)**, 908–933.

Souza, J., C. de Boyer Montégut, and P.-Y. Le Traon, 2011: Comparison between three implementations of automatic identification algorithms for the quantification and characterization of mesoscale eddies in the South Atlantic Ocean. *Ocean Science*, **7 (3)**, 317–334.

Taupier-Letage, I., I. Puillat, C. Millot, and P. Raimbault, 2003: Biological response to mesoscale eddies in the Algerian Basin. *Journal of Geophysical Research: Oceans*, **108 (C8)**.

Taylor, J. R., and A. F. Thompson, 2023: Submesoscale dynamics in the upper ocean. *Annual Review of Fluid Mechanics*, **55**, 103–127.

Tourbillon, L. G., 1983: The Tourbillon experiment: a study of a mesoscale eddy in the eastern North Atlantic. *Deep Sea Research Part A. Oceanographic Research Papers*, **30 (5)**, 475–511.

Tzortzis, R., and Coauthors, 2021: Impact of moderately energetic fine-scale dynamics on the phytoplankton community structure in the western Mediterranean Sea. *Biogeosciences*, **18 (24)**, 6455–6477.

Tzortzis, R., and Coauthors, 2023: The contrasted phytoplankton dynamics across a frontal system in the southwestern Mediterranean Sea. *Biogeosciences*, **20 (16)**, 3491–3508.

Van Sebille, E., and Coauthors, 2018: Lagrangian ocean analysis: Fundamentals and practices. *Ocean Modelling*, **121**, 49–75.

Wang, Z., G. Chen, C. Ma, and Y. Liu, 2023: Southwestern Atlantic ocean fronts detected from the fusion of multi-source remote sensing data by a deep learning model. *Frontiers in Marine Science*, **10**, 1140 645.

Weiss, J., 1991: The dynamics of enstrophy transfer in two-dimensional hydrodynamics. *Physica D: Nonlinear Phenomena*, **48 (2-3)**, 273–294.

671 Wyrtki, K., L. Magaard, and J. Hager, 1976: Eddy energy in the oceans. *Journal of Geophysical*
672 *Research*, **81 (15)**, 2641–2646.

673 Zhang, Z., B. Qiu, P. Klein, and S. Travis, 2019: The influence of geostrophic strain on oceanic
674 ageostrophic motion and surface chlorophyll. *Nature Communications*, **10 (1)**, 2838.

675 Zhang, Z., W. Wang, and B. Qiu, 2014: Oceanic mass transport by mesoscale eddies. *Science*,
676 **345 (6194)**, 322–324.